CAAP Quarterly Report

[09/27/2023]

Project Name: "All-in-One Multifunctional Cured-In-Place Structural Liner for Rehabilitating of Aging Cast Iron Pipelines"

Contract Number: 693JK32250009CAAP

Prime University: North Dakota State University

Prepared By: [Ying Huang, ying.huang@ndsu.edu, 701-231-7651]

Reporting Period: [07/01/2023 – 09/27/2023]

Project Activities for Reporting Period:

In the 3rd quarterly report, Tasks 2.1, 3.1, 3.3, 3.4, and 4.1 were carried out as proposed. In this quarter (Quarter 4), the research team has consistent progress on Tasks 2.1, 3.1, 3.4, and 4.1, and also broadened their study on Tasks 2.2, 3.2, 4.2, and 5.1. The summaries of the key activities completed during the fourth reporting period are provided below.

Task 2.1 Preparation of Vitrimer Epoxy Resins, Characterization, and Optimization of the Processing and Curing Conditions (30%): During this reporting period, the research team (Dr. Long Jiang and Austin Knight, Ph. D. student from NDSU) performed a new modified formation for self-healing polymer to overcome the workability limitations presented in last report. The reaction mechanisms and formation developments are summarized below:

(1) Improving Self-healing & UV-Curable Adhesive Workability: A catalyst is required to increase the rate of methacrylation of the bisphenol an epoxy resin (BADGE) and to lower the temperature of and improve the self-healing properties of the cured adhesive. The catalyst selected for this role is methacrylate functional which allows the catalyst to be covalently bonded to the polymer structure after curing. However, this functional catalyst (FC) has been spontaneously polymerizing with the resin shortly after being added leading to a viscous resin with significant polymer chain interactions making it difficult to work with. Adding reactive diluent (RD) in a 0.5:1 to 1:1 functional group ratio allowed for the FC polymer to be dissolved resulting in a low viscosity resin. However, when adding additional FC to improve the self-healing properties the polymer came out of solution causing the resin to greatly increase in viscosity again. For this reason, the FC was replaced with a non-functional catalyst (NFC). Since this catalyst is non-functional, it does not covalently bond with the polymer and may act as a plasticizer in the resin once additional catalyst is added to improve the self-healing properties. If the NFC decreases the resin's properties too much, another option that can be tested is to incorporate an inhibitor to try and prevent the spontaneous polymerization of the FC.

Task 2.2 Investigating Self-healing and Mechanical properties of Vitrimer Epoxy Resins (20%): During this reporting period, the research team (Dr. L. Jiang, Dr. Y. Huang, and Austin Knight, Ph. D. student from NDSU) investigated the self-healing and mechanical performances of the vitrimer epoxy resins in Subtask 2.1, a series of self-healing and tensile properties tests were conducted, and the results are presented below:

(1) Self-healing Testing to Optimize the Healing Conditions: The self-healing reaction of the UV-curable resin is activated at elevated temperatures and requires some pressure to mold two pieces together or fill cracks. Fractured tensile samples were adhered to each other at 150°C for 1 minute using a vice plier to apply pressure (Figure 1). Three formulations were tested: the base resin (0.01FC), the resin with 1:1 methacrylic reactive diluent (0.01FC 1MRD), and the resin with 1:1

methacrylic reactive diluent and 0.1:1 functional catalyst (0.1FC 1MRD). All three formulations adhered well and were unable to be separated at the point of adhesion and broke elsewhere when pulled apart. This signifies that a strong bond was formed during the self-healing process, but it is still necessary to obtain more quantitative results to compare formulations by mechanically testing, self-healing, and then retesting specimens.

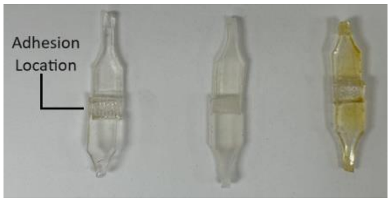

Figure 1. The adhesion of tensile specimens of 0.01FC (left), 0.01FC 1MRD (middle), and 0.1FC 1MRD (right).

(2) Self-healing Process: Cracks were also cut into the surface of the 0.01FC 1RD formulation and then healed at 150°C for 5 minutes at 50psi in a hot press. Topographical images of the crack surface were taken before and after healing using an optical microscope to compare the change in the crack depth (Figure 2). After healing, the crack depth was reduced from 450 to 120µm. When hot pressing the self-healing polymer, the polymer would spread out considerably. Confining the edges of the sample when self-healing to prevent this will allow the polymer to heal cracks more efficiently and mimic the field conditions of the self-healing of the liner more closely.

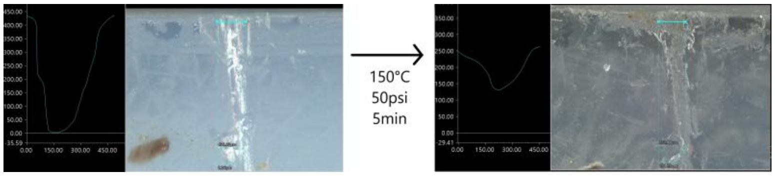

Figure 2. Topographical images before and after healing the self-healing polymer.

(3) Tensile Properties of Self-Healing UV-Curable Adhesive: Tensile testing was performed on the base formulation, 0.5:1 methacrylic reactive diluent (MRD), and 1:1 MRD. With increasing MRD concentration, the strength, strain, modulus, and toughness all increased. The strength and modulus of the self-healing resin are less than that of the commercial resin while the strain and toughness are higher.

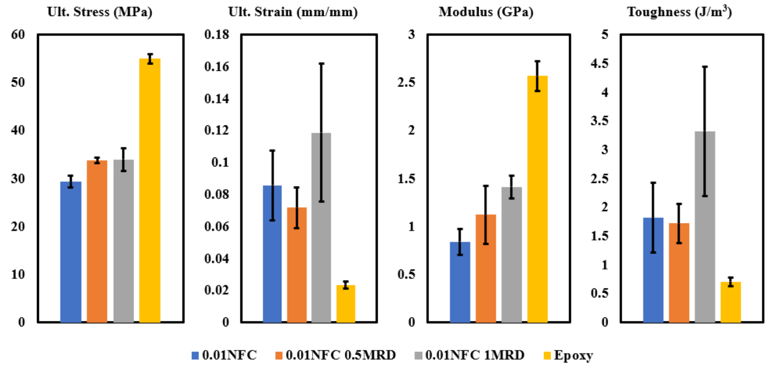

Figure 3. A summary of the tensile properties of the self-healing UV-curable resin compared to a commercial two-part epoxy system.

Task 3.1 High Mechanical Performance (10%): During this reporting period, the research team (Dr. Ying Huang, Dr. Zhibin Lin, Dr. Xingyu Wang, and Muhammad Imran Khan, Master student from NDSU) conducted experimental studies on nanoparticle reinforcement, specifically on the flexural properties. The investigations and their key findings are provided below:

(1) Continuing with previous study, study in this period focuses on evaluating the influence of nanoparticles on the flexural properties of polymeric composite. Consistent with previous study, the nanoparticles including carbon nanotubes (CNT), graphene nanoplatelets (GNP), and

nanodiamonds (ND). It can be seen from Figure 4 that the optimal concentration for these investigated nanoparticles is between 0.5 to 1.0 wt.%.

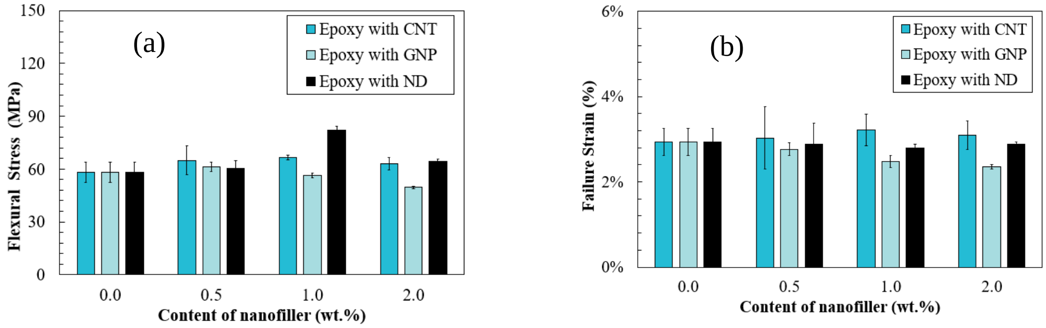

Figure 4. Flexural properties of neat epoxy with and without nanoparticle reinforcement. (a) flexural strength, (b) failure strain.

Task 3.2 Enhanced Bonding Performance (10%): During this reporting period, the research team (Dr. Ying Huang, Dr. Xingyu Wang, and Muhammad Imran Khan, Master student) conducted an experimental study on nanoparticle reinforced adhesive interfacial bonding strength between adhesives and substrate. The investigations and their key findings are provided below:

(1) Continuing with previous study, study in this period focuses on evaluating the influence of nanoparticles on the shear bonding properties. Figures 5 show the testing results for the flexural properties with epoxy composite reinforced with CNT, GNP, and ND. It can be seen that the optimal concentration for these investigated nanoparticles is between 0.5 to 1.0 wt.%.

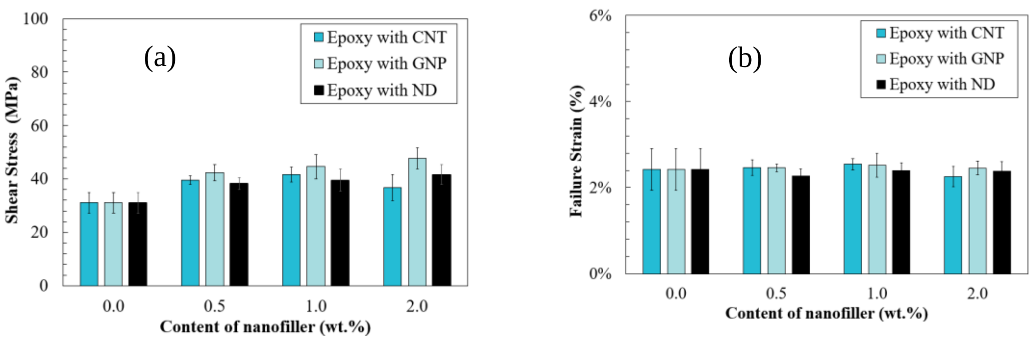

Figure 5. Single Lap Joint adhesion of neat epoxy with and without nanoparticle reinforcement. (a) shear strength, (b)failure strain.

Task 3.3. Reducing the Permeability and Investigating the Interfacial Bonding Chemical Analysis (20%): During this reporting period, the research team (Dr. Liangliang Huang, Qiuhao Chang, Ph. D. student from University of Oklahoma) have conducted studies on developing computational models for the evaluating hydrogen models based on their density and self-diffusion properties.

(1) During this reporting period, we evaluated rigid pore models and investigated pore chemistry effect on the self-diffusion of hydrogen in pores; and the utilized model is presented in Figure 6.
(2) Results and findings: As presented in Figure 7, at low pressures, self-diffusion coefficients demonstrate that H2 diffusion is faster in graphene pores than in kaolinite nanopores, despite H2 having stronger attractive intermolecular interactions with graphene. Lateral VACF results reveal a faster decay time for H2 molecules in kaolinite, suggesting that H2 molecules have more collisions with the kaolinite surface than the graphene surface. So, slower self-diffusion in kaolinite may be explained by greater surface roughness.

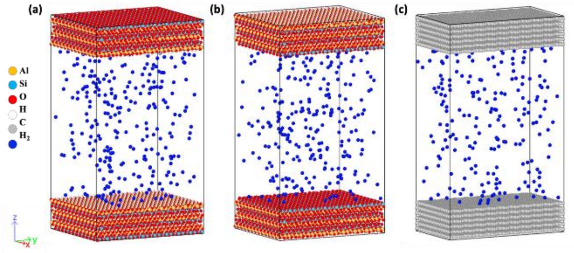

Figure 6. Hydrogen molecules confined in 3 types of nanopores. (a) Kaolinite pore with inward-facing AlO4(OH)2 surface. (b) Kaolinite pore with inward-facing SiO4 surface. (c) Graphene pore.

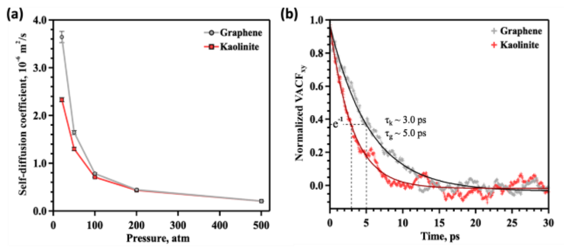

Figure 7. Diffusion behavior of H2 in 2 nm kaolinite (Al surface) and graphene pores. (a) Total self-diffusion coefficients at pressures ranging from 20-500 atm. (b) Normalized lateral velocity autocorrelation functions at P = 20 atm.

Task 3.4 Finite Element Numerical Analysis to Guide the Design of the Developed high-performance healable CIPP Structural Liner (30%): During this reporting period, the research team (Dr. Chengcheng Tao, Junyi Duan, and Yizhou Lin, Ph.D. students from Purdue University) have conducted finite element analysis (FEA) for flexural properties of epoxy samples as summarized below:

(1) FEA Model Setup: We created three-dimensional (3D) FEA model in Abaqus to simulate the three-point bending test performed in the laboratory. In accordance with the experimental results, the samples failed at displacements of 5.5 mm and 7 mm in negative Y direction respectively. Therefore, an identical displacement control is applied on the reference point, situated at the center of the crosshead. We also implement finer mesh refinements in the central area of the sample. The FEA neat epoxy sample model with mesh is shown in Figure 8.

(2) Results and Discussion: The flexural stress-strain curves derived from both experimental and simulation outcomes are plotted in Figure 8. It is shown that the accuracy of the ultimate stress prediction by FEA is 99% for sample 1 and 97% for sample 2. Furthermore, minor deviations are inevitable during the flexural tests, due to manual pouring and the sample surface are not absolutely smooth. Overall, the FEA well predicts the three-point bending performance of neat epoxy trial samples, which can be used as a reliable tool for further sensitivity studies.

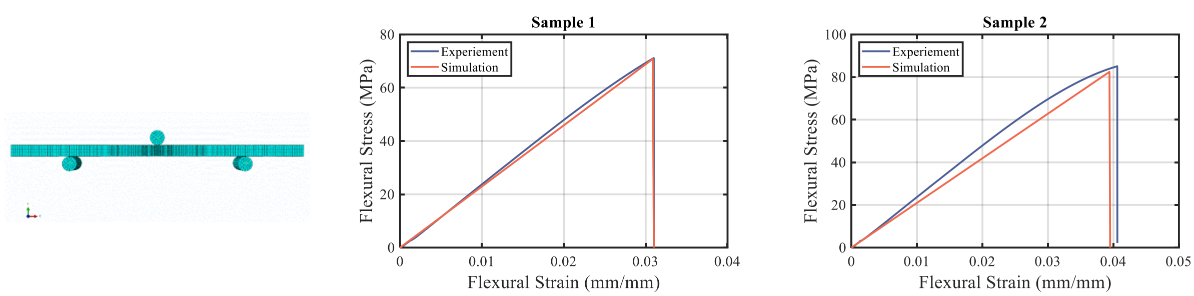

(a) (b) (c)

Figure 8. (a) FE model with mesh and (b) (c) Comparison of three-point bending test results

Task 4.1 Development of Embedded Distributed Fiber Optic Sensors for Self-sensing Structural Liner (10%): During this reporting period, the research team (Dr. Ying Huang, and Dr. Xingyu Wang) conducted an experimental study on corporation distributed fiber optic sensors to polymeric composite, the major findings are presented below:

(1) In this study, we explored the integration of distributed optical fiber sensors into composite materials, with a particular focus on structural liner systems. An optical sensor was embedded within a 12x2-inch CIPP liner specimen (as shown in Figure 8(a)), serving to monitor internal strain during the curing process.

(2) Figure 8(b) presents the evolution of curing strain on the steel surface over a span of 36 hours. To gain a more nuanced understanding of the curing process, we conducted internal curing strain measurements at two specific locations, denoted as Point 1 and Point 2, as illustrated in Figure 9(c). The strain development at Point 2 is particularly noteworthy, as it exhibited a positive strain, could be attributed to the shrinkage of the adjacent epoxy, resulting in an unusual strain pattern. Consequently, this area may be susceptible to cracking before other surface areas. Figure 9(d) further emphasizes the significance of our findings by pinpointing potential vulnerable zones within the liner.

(3) Figure 8(e) displays the curing strain observed on the inner surface of the CIPP liner (fabric surface). The results clearly illustrate a notable disparity between the curing strain experienced on the fabric surface compared to the steel substrate. Importantly, the strain development on the fabric surface exhibits significantly higher magnitudes, encompassing both negative and positive strain values, when contrasted with the steel surface.

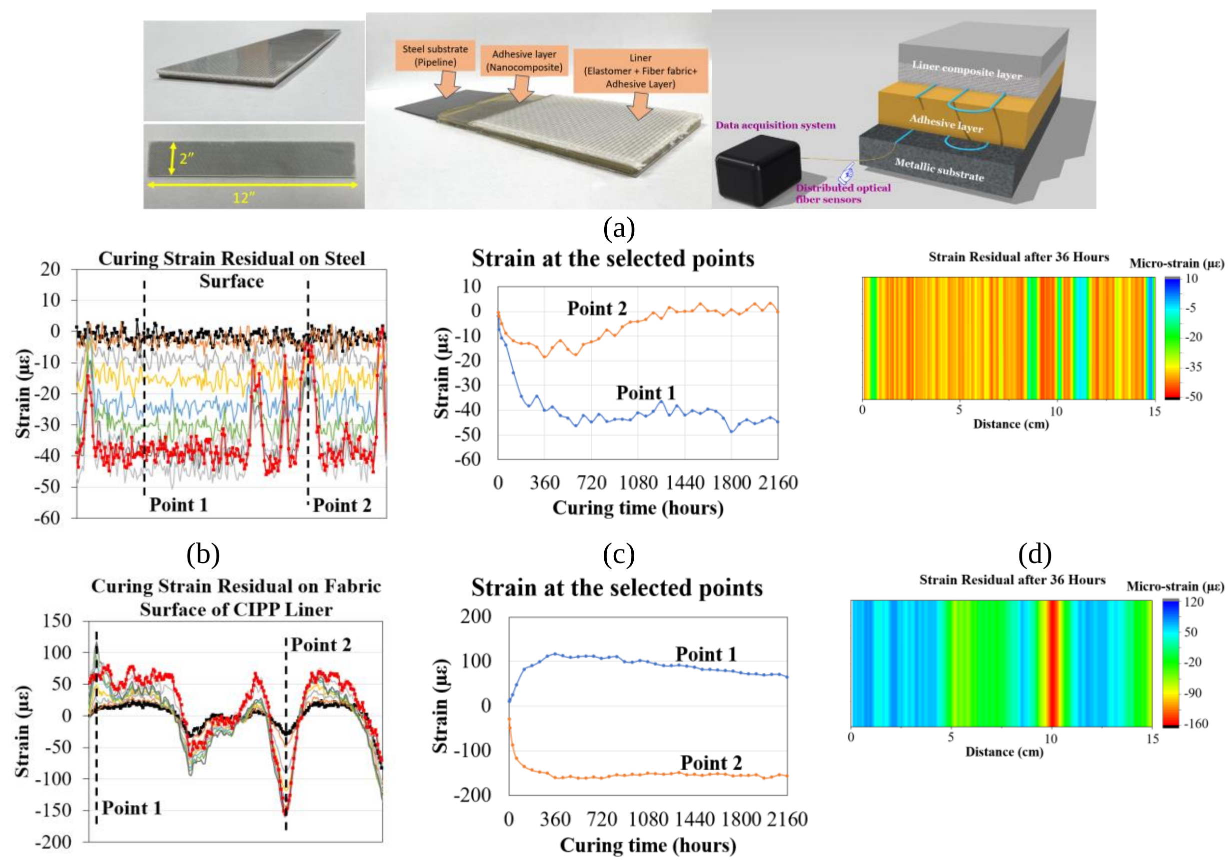

Figure 9. (a) Illutration of the CIPP sample with distributed fiber optic sensors, internal strain on (b)(c)(d) steel surface, and (e)(f)(g) CIPP liner surface.

Task 4.2 Investigating the load transfer between layers of the CIPP liner and the cast-iron substrate (10%): During this reporting period, the research team (Dr. Ying Huang, and Dr. Xingyu Wang) conducted an experimental study on corporation distributed fiber optic sensors to the CIPP liner, the major findings are presented below:

(1) This study examined the integration of distributed optical fiber sensors into a CIPP liner and assessed the strain/load transfer between the layers of the CIPP liner and the steel substrate. Figure 9(a) illustrates the experimental setup, while the results for steel and the CIPP liner are presented in Figure 10(b) and (c), respectively. Evidently, under identical bending displacements, there can be significant variation in the strain development between the CIPP liner and the steel substrate. These findings can provide valuable insights for the research team in understanding the relationship between collected strain values in the CIPP liner and the steel substrate.

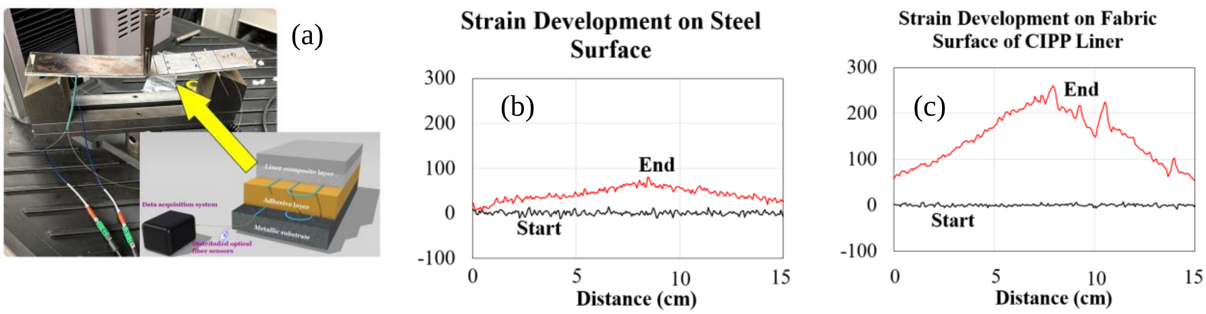

Figure 10. (a) Illutration of the CIPP sample with distributed fiber optic sensors, strain development under displacement on (b) steel surface, and (c) CIPP liner surface.

Task 5.1 Development of CIPP liner risk index for the pipeline integrity management enhanced by AI algorithms (20%): During this period, the research team (Dr. Chengcheng Tao, and Junyi Duan Ph.D. students from Purdue University) have conducted machine learning-based risk model for pipeline integrity management, the findings are presented below:

(1) Model groups: The correlation map for ten different variables is plotted in **Error! Reference source not found.**. The map illustrates the relationship between these nine factors (input) and failure type (output). The factors are ranked according to the absolute value of the correlation coefficient from high to low as follows: “Facility”, “Leak detection”, “Age years”, “Pipe diameter”, “Land use”, “Facility part”, “Gross”, “Service”, and “Net loss”.
(2) Results: Multivariable Linear Regression (MVLR) was utilized in data analysis, the results in Figure 11(b) show that 25% of testing data aligns well with the real values, with only 1.5% of the residual outliers. In addition, the distribution of residuals ranges from zero to one and matches the theoretical straight line well, indicating MVLR is a reliable machine learning algorithm for pipeline risk evaluation.

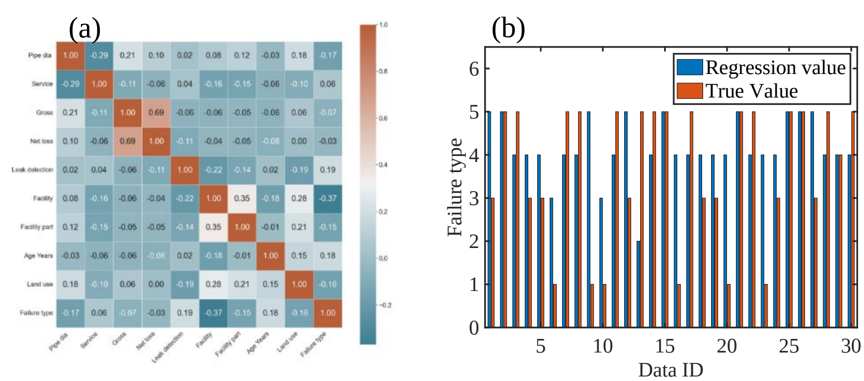

Figure 11. (a) Correlation map of pipeline variables (b) comparison between MVLR results and true

Project Financial Activities Incurred during the Reporting Period:

The cost breakdown during the reporting period in each category according to the budget proposal is shown in Table 1.

Table 1. Cost breakdown

Category	Amount spent during Q4
Personnel	
Faculty	$11323
Postdoc	$6120
Students (RA and UR)	$5940
Benefits	$5676
Operating Expenses	
Travel	$0
Materials and Supplies	$581
Recharge Center Fee	$353
Consultant Fee	$675
Subcontracts	$0
Indirect Costs	$13800

Project Activities with Cost Share Partners:

The Match fund from NDSU for this project is coming from the tuition of the associated graduate students during their work on this project. During the reporting period (Q2), Austin Knight, Zahoor Hussain, and Tofatun Jannet were hired on the project. The tuition for the three students during Q4 is estimated to be $10,891 at a rate of $463.73 per credit.

Project Activities with External Partners:

During this reporting period, George Ragula, our industry consultant, attended all the bi-weekly meetings with the research team and communicated with PPM and other industry partner obtaining liner testing samples for the research team.

Potential Project Risks:

No potential risks were noticed during this reporting period.

Future Project Work:

In the next quarter, the research team will continue working on Tasks 2.1, 2.2, 3.1, 3.2, 3.3, 3.4, 4.1, 4.2 and 5.1.

Potential Impacts on Pipeline Safety:

The findings regarding self-healing epoxy and high-performance nano-epoxy composites demonstrated their potential to enhance the safety of pipelines with CIPP liners. The results obtained from the CIPP liner equipped with sensors indicate that the distributed optical sensor can proficiently monitor the CIPP liner throughout its entire lifecycle, from the curing process to enduring mechanical deformation during its service life. Additionally, results from MVLR suggest that it is a reliable machine learning algorithm for pipeline risk evaluation.